(Received 21 December 2023, Accepted 26 January 2024, Scheduled 19 February 2024)

Advancing Microstrip Patch Antennas through Prosopis Africana Conductive Ink-Based Thick Films for Enhanced Bandwidth in Radar Applications

Suleiman Babani[1, 3], Mohd Nizar Hamidon[1, 2, *], Alyani Ismail[2], Haslina Jaafar[2], Intan Helina Hassan1[1], Jun Jiat Tiang[4], Surajo Muhammad[5], and Ibrahim Garba Shitu[1]

[1] *Institute of Nanoscience & Nanotechnology (ION2), Universiti Putra Malaysia, 43400 UPM Serdang, Selangor, Malaysia*
[2] *Faculty of Engineering, Universiti Putra Malaysia, 43400 UPM Serdang, Selangor, Malaysia*
[3] *Department of Electrical Engineering, Faculty of Engineering, Bayero Universiti Kano, PMB 3011 Kano, Nigeria*
[4] *Centre for Wireless Technology, Faculty of Engineering, Multimedia University, Cyberjaya 63100, Malaysia*
[5] *Futurist Unit, Innovation & Portfolio Management Division, TM Innovation Center Lingkaran Teknokrat Timur, Cyberjaya 63000, Malaysia*

ABSTRACT: This paper addresses the bandwidth limitations inherent in microstrip patch antennas, which are commonly employed in radar applications owing to their compact size and integration convenience. To overcome these limitations, this study explores the application of Prosopis Africana conductive ink-based thick film, an innovative and environmentally friendly material. Originating from the African mesquite tree, this ink exhibits high conductivity owing to its elevated carbon content, presenting a compelling solution for enhancing microstrip patch antenna bandwidth. The research entails thoroughly examining microstrip antenna design principles and associated challenges, followed by exploring the unique properties of Prosopis Africana conductive ink. A detailed methodology outlines the fabrication process of the ink-based thick layer or film on the substrate, with simulation and measurements employed to evaluate its impact on impedance matching and radiation characteristics. Emphasizing the eco-friendliness of Prosopis Africana conductive ink aligning with green electronics trends, the study showcases its potential for advancing wireless communication systems while reducing ecological footprints. Results demonstrate a substantial bandwidth improvement exceeding 1.85 GHz, a simulation $|S_{11}|$ return loss value of -16.19 dB, and achieved 84.5% radiation efficiency of the operating frequency at 9.5 GHz and a peak realized gain of 7.10 dB. Hence, integrating Prosopis Africana conductive ink-based thick film is a viable strategy for augmenting microstrip patch antenna bandwidth, rendering them more adept for radar applications.

1. INTRODUCTION

Antennas play a crucial role in radar and wireless communication systems because they act as a link between electromagnetic waves and digital domain [1, 2]. Microstrip patch antennas (MPAs) have become increasingly popular among various antenna options due to their compact size, easy production, and versatility across different applications [3]. One of modern antenna design's biggest challenges is expanding the bandwidth while ensuring efficient performance [4]. The need for broader bandwidth arises from the ever-increasing demand for high-speed data transfer, multifunctional radar systems [5], and the complex requirements of wireless communication standards [6]. To tackle the challenge of expanding the boundaries of antenna technology, scientists and engineers are exploring new materials and fabrication techniques. One innovative approach involves using conductive inks derived from natural sources, such as Prosopis Africana, to create thick films as a unique antenna substrate. This pioneering strategy combines the benefits of microstrip patch antennas with the exceptional properties of Prosopis Africana conductive ink. It provides a solution to the bandwidth enhancement challenge in radar applications [7, 8]. Prosopis Africana is a plant native to Africa and has been traditionally used in various fields [9]. They include traditional medicine [10], woodworking [11], livestock feed [12], water treatment [13], and high carbon-based content [14]. Recent research has uncovered its potential use in conductive materials. Specifically, it has been found to have excellent electrical conductivity and dielectric properties [15]. Prosopis Africana conductive ink in the production of thick film fabrication presents an exciting path for improving the bandwidth of microstrip patch antennas. This is particularly important in radar systems for surveillance, communication, weather forecasting, and other related applications. Our research focuses on using Prosopis Africana conductive ink-based thick films as substrates for microstrip patch antennas. Our primary goal is to enhance the bandwidth characteristics of these antennas, which in turn will improve data throughput and radar system capabilities. This will lead to better resolution, target discrimination, and overall performance. By using this sustainable and eco-friendly material, we can contribute to developing environmentally conscious antenna technologies. Thick film technology emerges as a promising solution for MPA fabrication, offering versatility in substrate selection and a range of thick layer pastes with customizable electrical characteris-

* Corresponding author: Mohd Nizar Hamidon (mnh@upm.edu.my).

tics, and dielectric to match desired performance criteria [16]. However, conservative conductive thick layer pastes like copper and silver pastes pose challenges in parameter control for MPAs. Additionally, the utilization of copper paste is suboptimal due to its susceptibility to oxidation under ambient room temperature conditions. This study introduces an innovative thick-film paste incorporating nanoscale Prosopis Africana Char (PAC) powder and an organic vehicle (O.V.) derived from linseed oil (L.O.), marking a novel contribution to the field. This novel thick-film paste, hitherto unreported, facilitates microstrip patch antenna performance enhancement using a common FR-4 substrate. Additionally, applying thick film technology offers ease of fabrication, allowing for the precise screen printing of the prepared thick film paste onto various substrates as desired [17, 18]. This study explores the theoretical basis of microstrip patch antennas, explains the distinctive features of Prosopis Africana conductive ink, describes the process of fabricating thick film substrates, and outlines the methods used to increase antenna bandwidth. The potential benefits and applications of these antennas in radar systems are also discussed, making them more adaptable to the demands of modern communication and sensing technologies. This investigation represents a significant step to developing microstrip patch antennas with enhanced bandwidth. It paves the way for more advanced radar applications better suited to the changing needs of our world. As we embark on this journey of exploration and innovation, the results of this research will inspire further developments in antenna design and materials science, leading to more efficient and sustainable wireless communication and radar systems.

The contributions of the current work, to the best of our knowledge, include the following:

- Innovative Use of Prosopis Africana Conductive Ink: The paper introduces a pioneering application of Prosopis Africana conductive ink, derived from the African mesquite tree, as a conductive material for thick film fabrication in microstrip patch antennas.

- Overcoming Bandwidth Limitations: The primary contribution lies in addressing the inherent bandwidth limitations of microstrip patch antennas commonly utilized in radar applications. The study demonstrates that Prosopis Africana conductive ink substantially enhances the antenna's bandwidth, exceeding 1.85 GHz.

- Detailed Methodology and Fabrication Process: The paper provides a comprehensive methodology for fabricating the ink-based thick film on the antenna substrate. Simulations and measurements are employed to evaluate the impact on impedance matching and radiation characteristics.

- Eco-Friendly Approach: Emphasizing eco-friendliness, the research aligns with green electronics trends by showcasing the potential of Prosopis Africana conductive ink to advance wireless communication systems while contributing to environmentally conscious antenna technologies.

- Novel Thick-Film Paste: The study introduces a previously unreported thick-film paste incorporating nanoscale PAC powder and an organic vehicle derived from linseed oil. This innovative paste enhances microstrip patch antenna performance on a common FR4 substrate through screen printing.

- Electrical and Dielectric Properties Exploration: The paper sheds light on the unique electrical conductivity and dielectric properties of Prosopis Africana conductive ink. Traditionally used in various fields, this material emerges as a promising and eco-friendly alternative for conductive applications.

- Practical Production Method: The successful integration of Prosopis Africana conductive ink in thick film microstrip patch antennas on an FR4 substrate offers a suitable production method. This paves the way for enhanced antenna performance and more sustainable wireless communication and radar systems.

- The versatility of Thick Film Technology: Introducing a novel thick-film paste and ease of fabrication through screen printing adds to the versatility of thick film technology for MPA fabrication.

- Significant Advancement in Radar Technology: Overall, the research marks a notable advancement in exploring environmentally friendly materials for radar technology. The results and methodologies contribute significantly to developing microstrip patch antennas with improved bandwidth, addressing the evolving demands of modern communication and sensing technologies.

The subsequent segments of this manuscript are structured as follows. Section 2 delineates the method and material, while Section 3 provides an in-depth examination of the characterization of PAC thick film. Section 4 delves into the intricacies of microstrip patch antenna fabrication. The performance evaluation for PAC is comprehensively expounded upon in Section 5, encompassing rheology, thermal properties, surface morphology, dielectric and magnetic properties, including permittivity, dielectric loss tangent, and permeability. Section 5 further expounds on the simulated and fabricated microstrip patch antenna simulation prototype using PAC. Finally, the culmination of this study is encapsulated in Section 6, offering conclusive insights into the undertaken work.

2. MATERIALS AND METHOD

In this research, the raw biomass material under investigation was sourced from Prosopis Africana, a plentiful plant species in northern Nigeria. Specifically, the raw materials were collected from various farms within the Kafin Hausa Local Government Area of Jigawa State, Nigeria. The PAC was obtained through controlled pyrolysis of Prosopis Africana wood. The wood was subjected to pyrolysis at optimized temperatures and durations to yield PAC with the desired properties. The material was crushed with mortar and pestle into powder form and then later milled for 3 hrs using a milling machine SPEX08000D, where a ball-to-powder ratio (BPR) of 10 : 1 was employed to make the

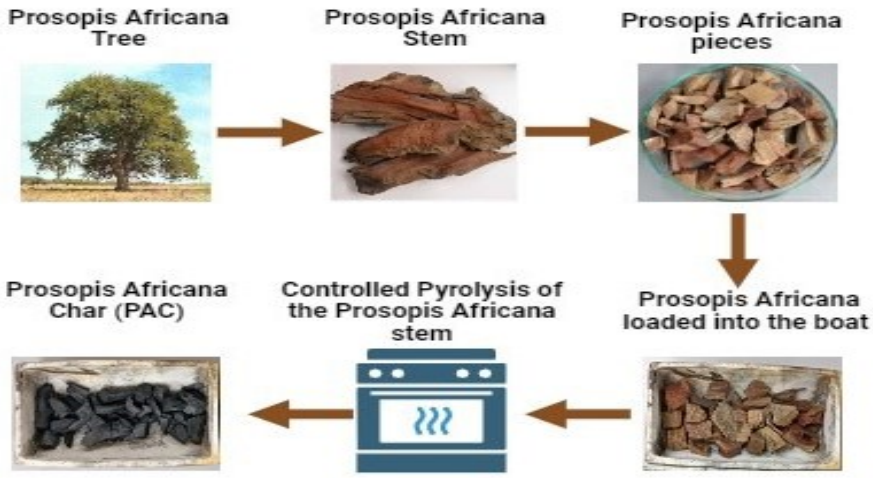

FIGURE 1. Step-by-step pyrolysis of Prosopis Africana Char (PAC) synthesis.

nanoparticles of the PAC to be used as the active material powder in the thick film antenna fabrication process, and the process is shown in Figure 1 [19]. The following chemical reagent substances were used in this study: (L.O.) (CAS No. The primary component (677466-08-1, Daler-Rowney). M-xylene (M.X) (CAS No. 1088-38-3, Sigma-Aldrich USA, Reagent Plus grade, 99% assay), and α-terpineol ($\alpha \cdot$ T) (CAS No. 104482-56-1, Sigma-Aldrich USA, natural, $\geq$ 96% assay) [16]. No changes were made to the chemicals after purchase. In the formulation of the paste, the initial step involved preparing the (O.V.) Specifically, 12.5 wt% of m.x and 85 wt% of L.O. were mixed utilizing a magnetic stirrer operating at 250 rpm for a duration of 3 hours. Following this, an additional 2.5 wt% of α·T was incorporated into the mixture, and stirring was prolonged for an additional 2 hours. Throughout the process, a constant of 40°C temperature was kept. The selection of component weight ratios for the organic vehicle was guided by prior investigations conducted by [20].

Subsequently, the previously formulated O.V. was introduced into PAC nanopowder at a weight ratio optimized under preliminary research. This amalgamation was subject to meticulous mixing through sonication, with a total duration of 1 hour, incorporating 10-minute intervals commencing after the initial 30 minutes, thereby achieving a uniform paste suitable for thick film printing. The selection of sonication as the preferred mixing method at this stage was driven by the magnetic properties inherent in the nanopowder employed for thick film paste formulation, rendering a magnetic stirrer unsuitable to achieve effective dispersion, as shown in the process in Figure 2. The PAC paste's viscosity and rheological properties were assessed by subjecting it to characterization using an Anton-Paar Rheoplus MCR3301 rheometer. The evaluation involved:

- To determine the relationship between the shear rate and viscosity,
- Explicitly maintaining a constant shear rate of 100 s^{-1},
- Observing changes in viscosity in the 0.1 to 100 s^{-1} shear rate range.

Subsequently, thermal gravimetric analysis (TGA) was conducted using a TGA/DSC apparatus to explore the effect of temperature on the composition of the paste. The samples were placed in aluminum crucibles and subjected to a temperature ramp spanning from 25 to 1000°C within an airflow environment to ascertain the thermal behavior of the material.

3. PAC FILM CHARACTERIZATION

The prepared thick film paste was deposited onto an alumina substrate using the printing screening technique, as depicted in Figure 3. A frame of silk screen, featuring a designated geometric pattern, preferably in a square or rectangular configuration, was utilized to apply the thick film through a silk printing apparatus for subsequent characterization. Subsequently, the organized samples underwent an initial drying process at room temperature for 15 minutes, followed by firing at temperatures of 300°C for 1 hour. This process was conducted within an incinerator box apparatus to evaluate the adherence and printability of the paste with the substrate under varying firing temperatures.

Subsequent to the deposition of the paste onto the specified substrate, an examination of the structural morphology of the thick film material was conducted using a field emission scanning electron microscope (FESEM) apparatus. In divergence, elemental composition analysis of the paste was carried out utilizing energy dispersive X-ray (EDX) spectroscopy. To mitigate material charging effects, a gold layer was applied to the materials through a sputter coater prior to their positioning on the sample holder. The dielectric properties, encompassing permeability, permittivity, and loss tangent of the PAC powder materials, were assessed utilizing a Vector Network Analyzer (VNA HB4291P) across the frequency spectrum of 8 to 12 GHz within the X-band range. The PAC samples were mixed with a hardener agent on the X-band sample holder, with the thickness of the samples of 3 mm. Then, it was left to dry for two days and then was measured, and the values of permittivity, loss tangent, and permeability from the VNA were analyzed. We do not need permeability values since carbon is not a magnetic material. It

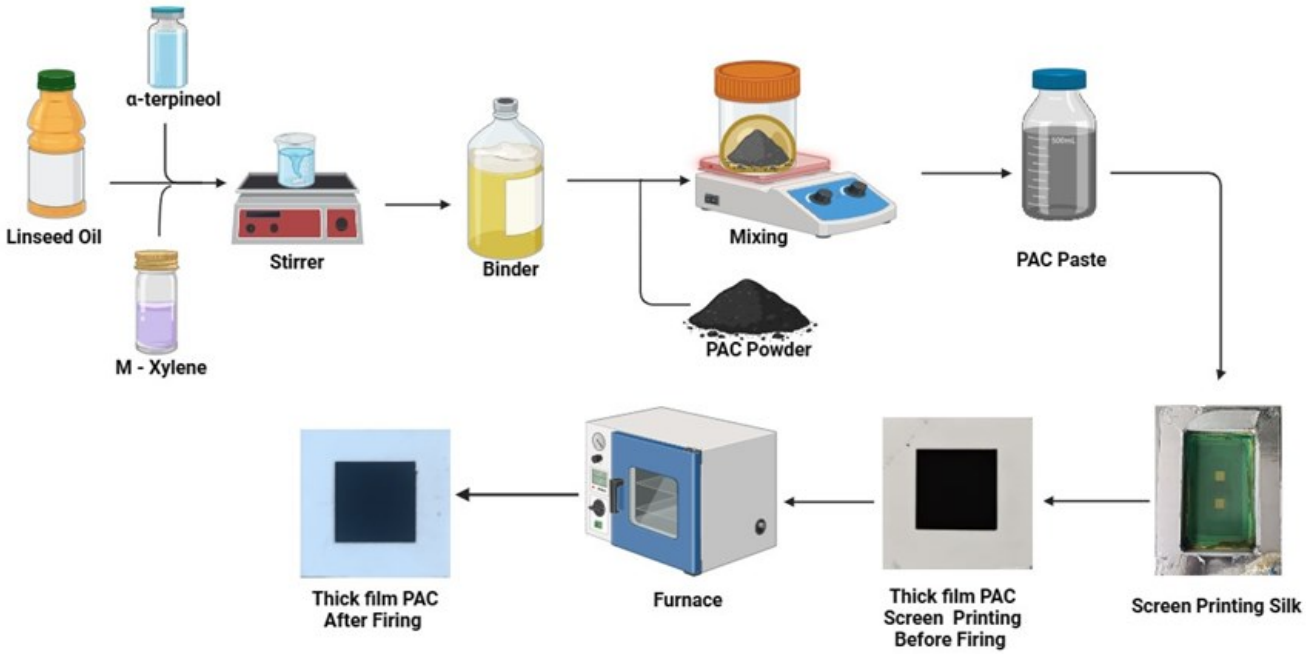

FIGURE 2. Preparation of O.V. and PAC paste thick film screen printing.

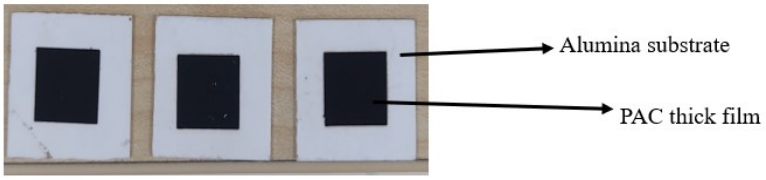

FIGURE 3. The characterization of the thick film of screen-printed PAC.

is worth noting that permeability data was not pursued due to the samples' non-magnetic nature of carbon content.

4. MICROSTRIP PATCH ANTENNA FABRICATION

Before commencing the fabrication process, preliminary simulations were imperative for formulating the design MPA parameters. Next, the antenna was tailored to function optimally within the 9.5 GHz frequency range, with a specific focus on its suitability for radar applications. The simulation phase was executed by applying CST software, a well-established tool in antenna design. The simulation employed a single-layer FR-4 substrate with an embedded copper layer on the other-sided ground. Following the finalization of the designs, they were then translated into a format suitable for stencil silk screen preparation. The production of the stencil screen encompassed a series of processes such as composition, exposing, and etching. Once the characterization of the thick film had been completed and appropriate viscous film parameters established, the creation of the MPA commenced. Subsequent to this, MPA was customized to exact specifications based on predetermined simulation results, and a Sub Miniature version A (SMA) connector was either soldered or attached to the antenna to facilitate measurements. Upon completion of the antenna fabrication procedure, the return loss and resonant frequency of all prepared samples with diverse parameters were evaluated using a VNA within the frequency range of 8 to 12 GHz. The experimental setup involved linking an MPA with an SMA connector fixed at the feed point to a cable establishing a connection with the S1 port. The primary measurement considered in this study pertained to $|S_{11}|$ parameters, denoting the magnitude of reflected power at the S1 port. To evaluate the performance of the patch antenna utilizing the PAC thick film, a comprehensive analysis was conducted, encompassing the examination of return loss, frequency shift, and antenna bandwidth.

5. DISCUSSION OF RESULTS

5.1. Rheological Properties

Figure 4 depicts the presented variation in the viscosity of the PAC paste at a consistent $100\,s^{-1}$ shear rate. The viscosity measurements were conducted for 10 minutes to observe the sustained alterations in viscosity over an extended time frame. The graphical representation demonstrates a consistent, gradual increase in viscosity across the PAC samples. Significantly, the rate of viscosity increase exhibits a relatively modest trend, signifying the sustained stability of the paste's viscosity throughout the observed period. The feature assumes paramount importance as it signifies the suitability of the paste for the printing

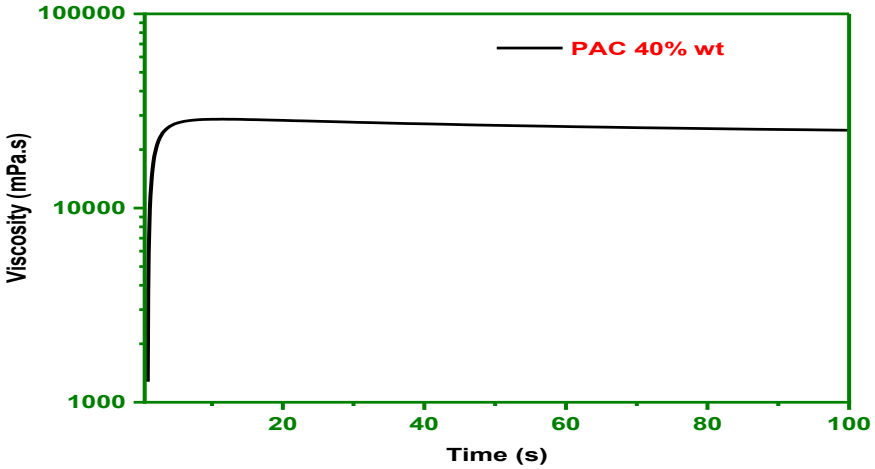

FIGURE 4. Measurement of the viscosity over time for PAC paste.

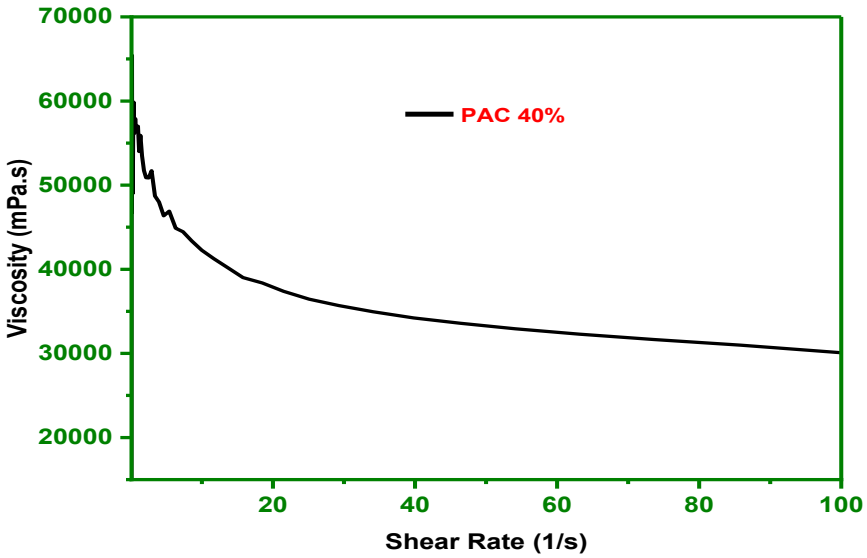

FIGURE 5. Measurement of the viscosity over shear rate for PAC paste.

process, as it ensures that the paste remains viable and does not excessively dry during its application to the silk screen frame or before passing through the mesh.

Throughout the screen-printing process, distinct phases of printing necessitate varied shear rates. As an illustration, as the paste moves through the aperture mesh within the frame, the shear rates may escalate, reaching nearly 98 s^{-1} [21]. Hence, it is crucial to acquire a comprehensive understanding of the variations in viscosity displayed by the PAC paste when being subjected to varying shear rates.

Figure 5 shows the relationship between the shear rate and viscosity, spanning 0.1 to 100 s^{-1}, enabling the observation of PAC viscosity trends associated with elevating shear rates. The PAC paste viscosity exhibits a consistent decline over the measurement range, commencing with a high viscosity level followed by a gradual reduction upon reaching 60 s^{-1}, and subsequently experiencing a rapid decline towards 100 s^{-1}. Hence, it is evident that pastes characterized by a weight ratio of 40% exhibit optimal suitability for the fabrication of thick films owing to their desirable rheological attributes. Notably, their ability to undergo a controlled reduction in viscosity under high shear rates is noteworthy. This reduction facilitates the smooth flow of the paste through the screen mesh during printing, promoting the creation of well-defined thick films on the substrate. Furthermore, once the printing operation concludes, the viscosity of the paste reverts to a higher level, thereby mitigating the risks of paste bleeding or smearing.

5.2. Thermal Analysis

To examine the impact of the firing conditions, specifically the temperature, and time on the PAC paste, the TGA was performed on the specimen. Figure 6 illustrates the percentage weight loss and decomposition rate, observed in the temperature range of 25 to 1000°C under an airflow atmosphere, with emphasis on the PAC paste. The commencement of volatile component evaporation from the paste occurred in the temper-

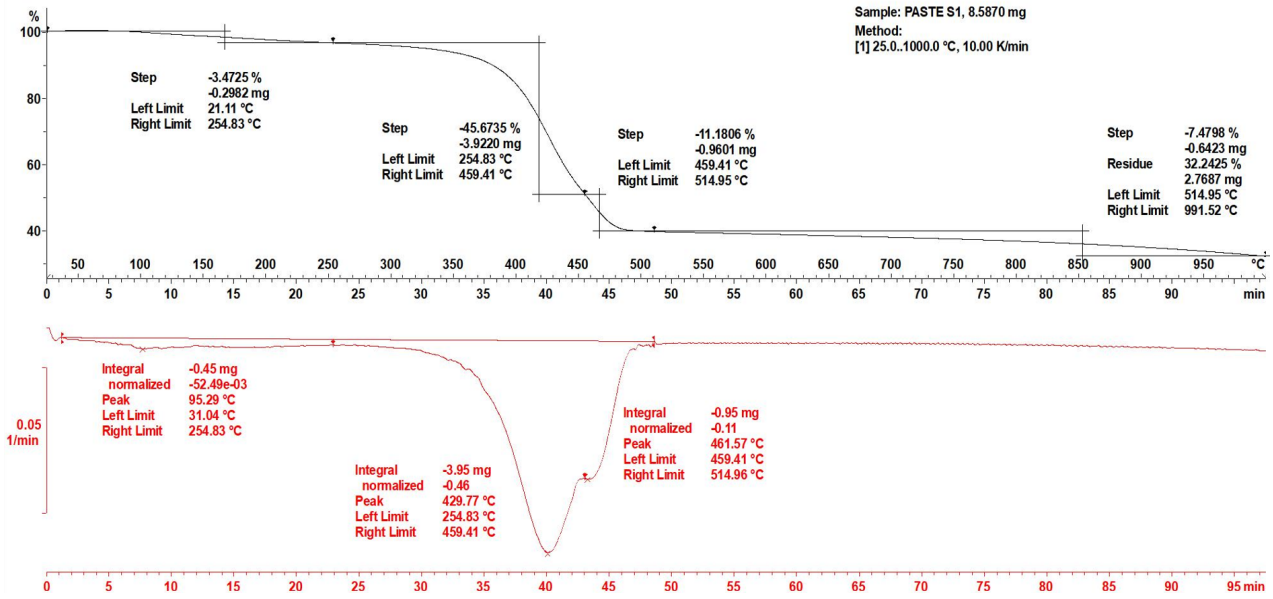

FIGURE 6. Weight loss and decomposition of PAC Paste.

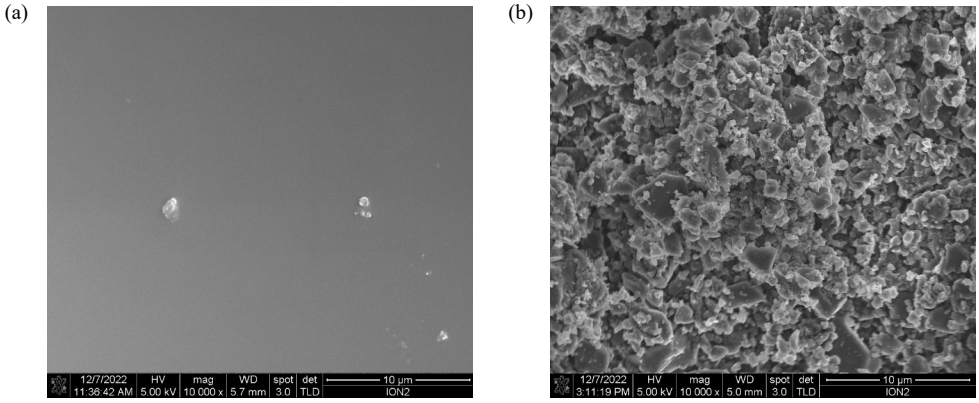

FIGURE 7. Morphology of PAC film at: (a) Room temperature and, (b) 300°C firing temperatures.

ature range between 50°C and 255°C. This range corresponds to the flash point and boiling point of M.X (25°, 138°) and α·T (90°, 217°), respectively [16]. Following this initial phase, the subsequent stage involved the elimination of non-volatile constituents, primarily the L.O. According to material specification documents, L.O. is characterized by a flashy theme of 300 °C, and a boiling theme exceeding 400°C. Notably, the vaporization of L.O. became prominent, with its boiling point reaching a maximum of 376 °C and beyond. A secondary decomposition event was ensued in the concluding stages of this thermal process, which transpired within the temperature range of 400 to 500°C. This phenomenon is directly associated with the breakdown of linseed oil, as by this stage, nearly all of the O.V. had volatilized and disintegrated and left the PAC ashes firmly adhered to the alumina substrate. Therefore, it can be deduced that the ideal temperature spectrum for PAC thick films, employing L.O. as its O.V. extends from 400 to 500°C. Within this spectrum, L.O. proves to be a suitable O.V. for formulating viscous films capable of withstanding lower firing temperatures.

5.3. Surface Morphology

The work expands its investigation to explore the influence of changes in firing temperature on the surface morphology of the PAC thick film. Specifically, two samples, one maintained at room temperature and the other subjected to a firing temperature of 300°C, were selected for detailed scrutiny. Figure 7 presents FESEM images and EDX analysis results of the PAC thick films after the firing process. Based on the findings presented in Figure 7(a), it is evident that the O.V., primarily L.O. based, has not undergone complete evaporation at ambient temperature, signifying that the surface remains coated with the residual O.V. In Figure 7(b), as the temperature is elevated to 300°C, the particles begin to manifest, although they are not yet distinctly discernible. The nanoparticles become distinctly visible only when being exposed to the firing temperature of

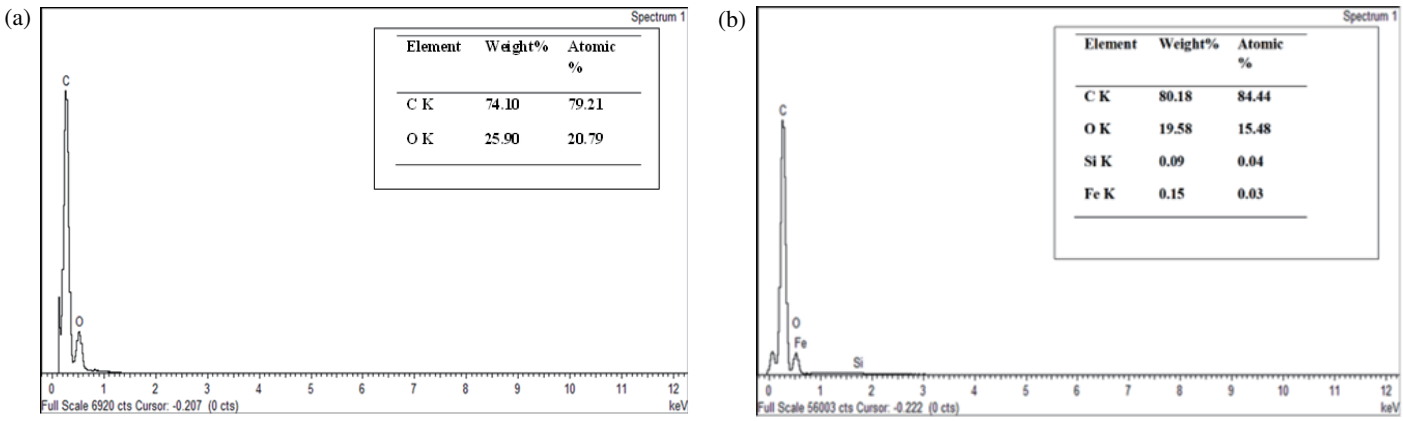

FIGURE 8. Elemental composition of PAC film at: (a) Room temperature and, (b) 300°C firing temperatures.

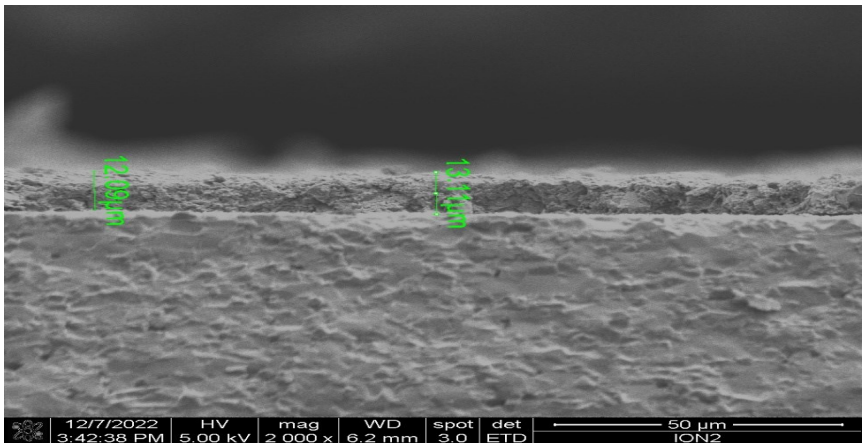

FIGURE 9. The cross-sectional view of the PAC film on the substrate.

300°C, and the dispersion of the powders becomes notably evident in the images [16]. One sample was used for conducting the Energy Dispersive X-ray (EDX) analysis, both at room temperature and after firing at 300°C. The EDX analysis was performed on the sample film under these two conditions and is presented in Figures 8(a) and 8(b). It was observed that the carbon component present in the O.V. decreased. At the same time, other elements associated with the PAC material began to increase as the firing temperature was raised. These EDX findings suggest that the elevated temperature led to the volatilization or desiccation of the organic binder, predominantly composed of L.O., allowing the nanoparticles beneath the oil layer to become exposed. In summary, the processed samples at 300°C revealed prominent nanoparticle visibility on the thick film's surface, which may influence the material's properties and overall performance. Notably, a relatively low firing temperature did not induce substantial alterations in grain growth or phase transformation in the initial materials. This observation suggests that the choice of firing temperature has no discernible impact on the microstructure or phase composition of the materials. Such findings will be of particular interest to researchers seeking to preserve their materials' original microstructure and phase properties [22]. Hence, both designated firing temperatures offer feasible choices for PAC film production, and the decision rests upon the maximal temperature compatibility of the chosen substrate utilized in the fabrication procedure.

Hence, the proposed work conducted a cross-sectional imaging on the PAC thick film to assess its thickness, adhesion, and uniformity of the paste layer on the substrate. As depicted in Figure 9, FESEM images were acquired to analyze the PAC thick film from a cross-sectional perspective, enabling an assessment of its adhesion, thickness, and dispersion on the substrate. The examination revealed that the PAC thick film exhibited a high degree of uniformity, with minimal voids, and presented a remarkably smooth surface, indicative of effective nanoparticle dispersion. Furthermore, the PAC film exhibited an exceptional bond with the substrate. Cross-sectional image analysis yielded a calculated thickness of approximately 13 μm for the PAC thick film, a dimension deemed suitable for thick film applications.

5.4. Characteristics of Dielectric and Magnetic Nature

The effectiveness of an MPA is intricately linked to the dielectric characteristics of its substrate, as emphasized in the intro-

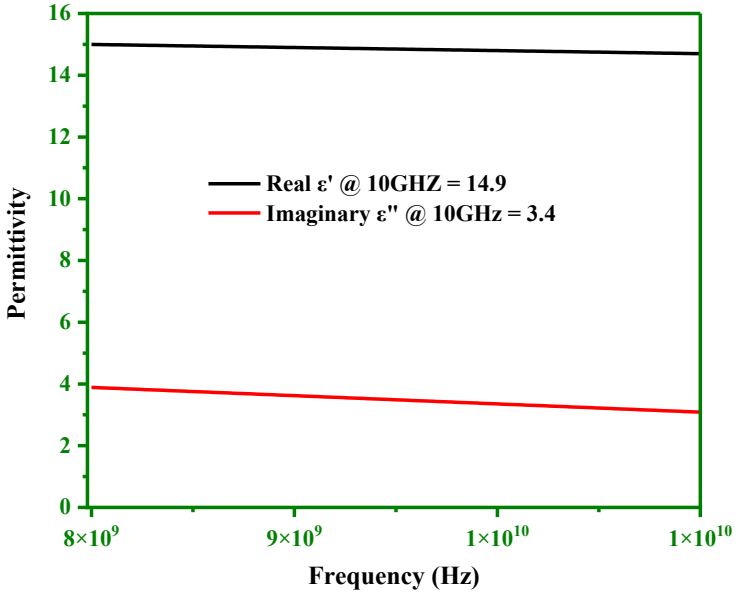

FIGURE 10. Real and imaginary permittivity of PAC thick film.

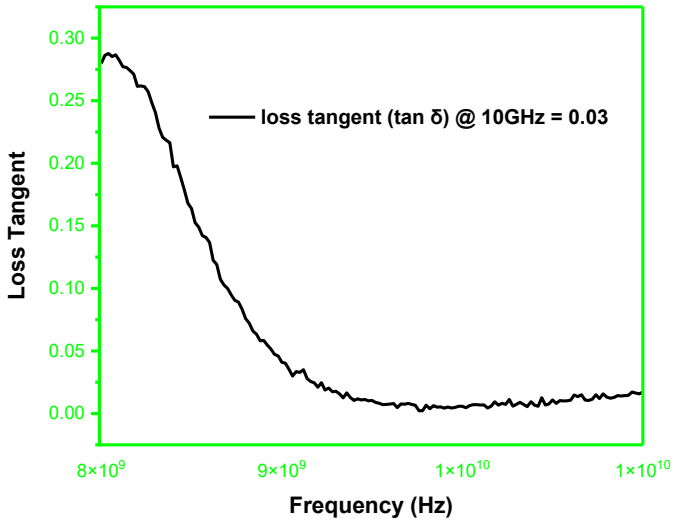

FIGURE 11. Loss tangent of PAC film.

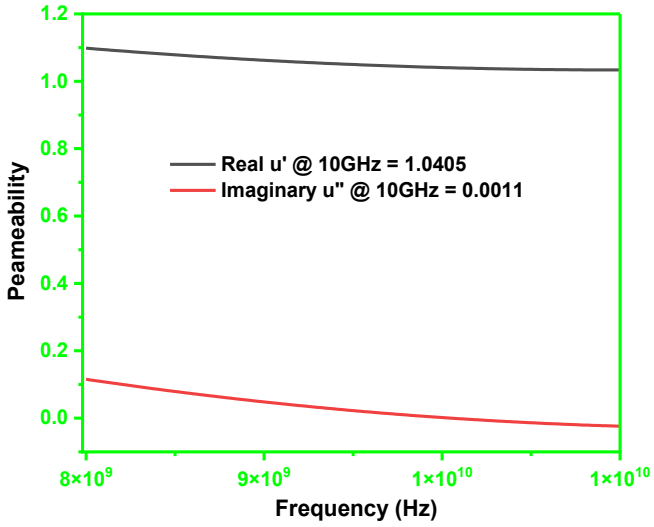

FIGURE 12. Real permeability of PAC thick film.

duction. Consequently, an essential aspect demanding investigation and analysis is the PAC thick film's dielectric behavior, which replaces conventional antenna substrates. The dielectric properties under scrutiny encompass parameters such as the permittivity, are often referred to as the dielectric constant and the dielectric loss tangent of the thick film. Using a VNA, these attributes can be quantified through measurement with an X-band sample holder.

5.4.1. Permittivity

Figure 10 presents a graphical representation of the actual and imaginary permittivity of the PAC thick film across a frequency range from 8 to 12 GHz. The obtained results reveal that the PAC thick film exhibits consistent permittivity values of $\varepsilon' = 14.9$ and $\varepsilon'' = 3.4$ at the frequency of 10 GHz, respectively. These values remained stable across the entire measured frequency spectrum. An exception is observed at frequency 10 GHz, with a noticeable permittivity constant from the initial values. Our findings have been cross-referenced with prior research [23], where difference materials in thick films but similar methods displayed reported permittivity values in the range of approximately 14 to 15, consistent with our present results. Additionally, [24] achieved a permittivity value of 14.4 for PAC, where the sample comprised nanopowders compacted into a sample holder with a thickness of 0.5 mm.

5.4.2. Loss Tangent (tan δ)

Figure 11 depicts the loss tangent (tan δ) of the PAC film. The tan δ, often called the dissipation factor (Df), exhibits a value of 0.03 at 10 GHz for the PAC thick film. This value falls within

TABLE 1. The dimensional values of the MPA.

Item	Calculated Value	Simulated Value
Permittivity (ε_r)	4.3	4.3
Length of the Patch, Lp (mm)	6.9	7
Width of the patch, Wp (mm)	9.6	9.5
Length of the Substrate, Ls (mm)	16.5	20.1
Width of the Substrate, Ws (mm)	19.3	10.3
Width of the Feeder, Wf (mm)	3.84	3.5
Thickness h (mm)	1.6	1.6

the range seen in FR4 substrates, which typically ranges from 0.03 to 0.05. However, this indicates that the PAC film can be categorized as a low-loss material suitable for antenna production. As depicted in Figure 11, it is evident that the loss tangent remains nearly constant, with minimal variation, for frequencies exceeding 10 GHz, a finding corroborated by [23].

5.4.3. Permeability

Figure 12 shows the permeability characteristics of the PAC thick film. At a frequency of 10 GHz, the real and imaginary permeability values for the PAC thick film are observed as 1.0405 and 0.0011, respectively. These findings align with established theory, indicating that permeability remains nearly constant at 10 GHz [23, 24]. Moreover, the PAC content within the thick film is relatively modest, accounting for 40 wt%. This observation of low permeability in the thick film corroborates previous research conducted by [23] on pristine or composite thick film. In [21], it is suggested that the presence of a non-magnetic material, such as an O.V. within the PAC film structure implies an anticipated low permeability due to the surrounding of nanoparticles by the organic binder. Under Snoek's rule, this low permeability typically correlates with a higher resonance frequency for the material. Thus, the thick film is anticipated to exhibit a relatively high resonance frequency compared to other materials.

5.5. Simulation of MPA

Prior to the fabrication of the MPA component, a simulation was conducted to determine the design parameters and dimensions for both the substrate and the radiating patch. Notably, even slight alterations in these dimensions can significantly impact the MPA's performance parameters. Hence, simulating the MPA is a critical preliminary step in the fabrication process. In accordance with the study's scope, the operational frequency of the MPA was established at 9.50 GHz, aligning with the X-band specifications outlined by ITU regulations. In the fabrication stage of this study, the substrate was chosen FR4 for investigation, and the simulation utilized PAC paste as the material for the feedline, and patch to define the dimensions of both the substrate and the patch. Dimensions of the radiating patch, represented by t for thickness and h for substrate height, are typically less than the wavelength. The width of the patch (W) can be determined using the formula below.

$$W = \frac{C}{2f_o\sqrt{\frac{\varepsilon_r+1}{2}}} \tag{1}$$

$$\varepsilon_{eff} = \frac{\varepsilon_r+1}{2} + \frac{\varepsilon_r-1}{2}\left[1+12\frac{h}{w}\right]^{-0.5} \tag{2}$$

$$\Delta L = 0.412h\frac{(\varepsilon_{eff}+0.3)\left(\frac{w}{h}+0.264\right)}{(\varepsilon_{eff}-0.264)\left(\frac{w}{h}+0.8\right)} \tag{3}$$

$$L = L_{\text{eff}} - 2\Delta L \tag{4}$$

By employing Equations (1)–(4) in conjunction with the substrate dimension computations as detailed the proportions simulation of the MPA and the characteristics of the FR4 substrate have been determined. The FR-4 substrate is characterized by a relative permittivity of 4.3 and has a thickness of 1.60 mm, the 0.035 mm thickness of copper, and the thickness of the conductive PAC is 0.01923 mm. After the parameter calculations are finalized, the subsequent step entails entering all dimensional data into the software (CST) and performing a simulation to verify the calculated frequency. Following the initial simulation, optimization was subsequently carried out through the parameter sweep functionality within the simulation to identify the maximum optimal parameters of the design. Each dimension is assigned variable values through parameter sweep, allowing for individual simulations with predefined parameter settings. The notable variance observed between theoretical calculations and simulation outcomes can be attributed to including various additional input parameters in the simulations. These parameters encompass the loss tangent, the electrical conductivity of the PAC material, the dielectric substrate, and the impedance matching of the microstrip feeder. A comparative analysis of MPA dimensions among calculated and simulated results is presented in Table 1.

In MPA simulating with FR-4 as the substrate, the post-optimization resonant frequency stands at 9.5 GHz, with an $|S_{11}|$ value of -21.85 dB. The simulation outcomes reveal that, in terms of the radiating patch dimensions, there was minimal deviation from the theoretically derived values. In the context of the FR-4 substrate dimensions, an exploratory sweep of parameters was executed to ascertain the optimal sizes. The analysis revealed notable variations in both length and width compared to the initial calculations. The observation underscores

TABLE 2. Summary of simulated and measurement value.

Parameters	Simulation Value	Measurement Value
Operating Frequency (GHz)	9.5	9.35
Return loss $\|S_{11}\|$ (dB)	-21.85	-16.19
BW @ -10 dB (GHz)	1.85	1.32
Peak Realization Gain (dB)	7.2	7.1

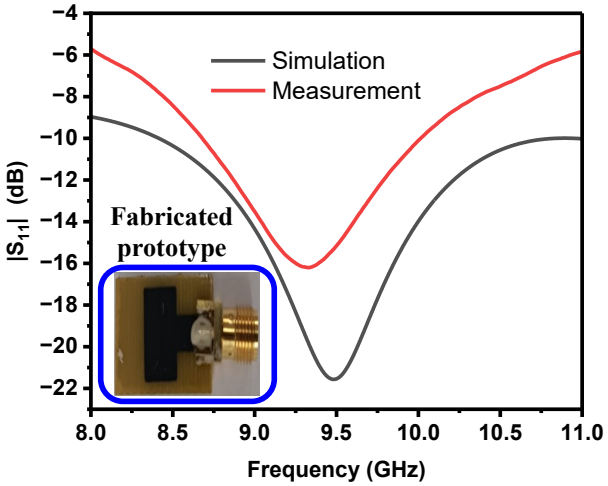

FIGURE 13. Simulation and measurement results of the proposed MPA using PAC films.

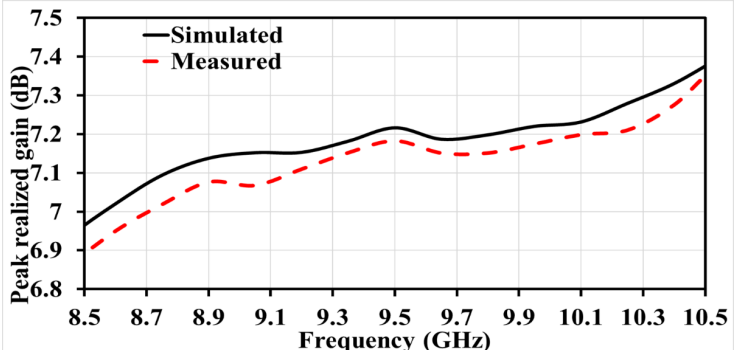

FIGURE 14. Simulated and measured of peak realized gain vs frequency.

the necessity of simulation for optimization and achieving more precise dimensional calculations, even if initial dimensions can be theoretically derived.

5.6. Fabrication and Measurement of the MPA

After the conclusion of the simulations, Magnetic Permeability Adjusters (MPAs) were manufactured using the screen-printing method. The PAC film on the FR-4 substrate was subjected to a firing temperature of 200°C, determined by the maximum thermal tolerance of the substrate. The visual representation of the manufactured MPA on the FR4 substrate is presented in Figure 13. The PAC thick film paste serves as the radiating patch, and the microstrip feedline is observed positioned on a single-sided FR-4 substrate. The frequency analysis covered a range from 8 to 11 GHz to assess the influence of the PAC thick film as a radiating patch at the previously simulated resonant frequency of 9.5 GHz. Figure 13 also presents the analysis of MPA performance with PAC thick film on an FR4 substrate within a frequency range of 8 to 11 GHz. Both simulation and experimental measurements were conducted to assess the impact of the PAC thick film as a conductive radiating patch on the simulated resonant frequency 9.5 GHz.

A detailed comparison between simulation and measurement results is provided, and a summary of all data is tabulated in Table 2. These findings reveal that the MPA fabricated with the PAC thick film significantly enhances return loss, bandwidth, and gain.

Figure 14 illustrates the variation in peak gain concerning frequency for the antenna under consideration. The graph com-

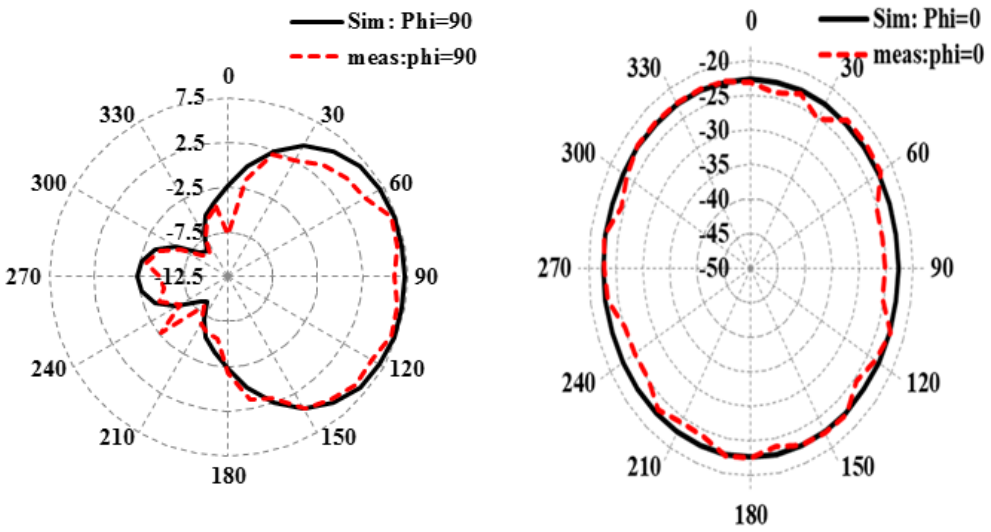

FIGURE 15. Simulated and measured radiation pattern.

TABLE 3. Comparison study of patch antenna over different carbon material with the previous work.

Ant	f_o (GHz)	Conductive Patch Material	$\|S_{11}\|$ (dB)	BW (GHz)	Gain (dB)	Application	Ref
R	10	MWCNT	-11.64	2.5	0.81	BW enhancement	[29]
R	2.45	NiZnFe/MWCNT	-22.03	1	-	ISM	[30]
R	5	Graphite	-17.63	0.297	-	Wireless Application	[31]
R	11.6	Graphene	-16.72	0.814	6.54	Military satellites	[32]
R	11.46	Graphene	-20.54	1.12	6.98	X and Ku band	[33]
R	15.04	Graphene	-12.05	1.45	–	5G	[34]
R	4.80	CNT	-17.50	0.99	–	Wireless body area network	[35]
R	6.296	SWCNT	-27.50	1.50	3.007	Detection COVID-19 Affected Lungs	[36]
R	3.7	Graphene	-31.00	0.5	3.17	Wearable Body Centric	[37]
This work	9.5	PAC	-21.5	1.85	7.2	Radar	

R = Rectangular Patch Antenna

prehensively analyzes the antenna's performance, showcasing the relationship between peak gain and frequency. Notably, the antenna achieves a maximum measured and simulated realized peak gain of 7.20 dB precisely at the targeted frequency of 9.5 GHz. This peak gain signifies the antenna's optimal efficiency and effectiveness within the specified frequency range, underscoring its suitability for applications demanding robust performance near 9.50 GHz. The observed consistency between measured and simulated results affirms the accuracy and reliability of the antenna's performance characteristics, validating its capability to operate with enhanced gain at the designated frequency.

Figure 15 illustrates a 2D radiation plot depicting frequency variations. The simulated and measured results are explicitly conducted at 9.5 GHz, offering insights into the radiation characteristics along two distinct planes: the xz-plane, defined by $(\psi = 0°|0° < \theta < 180°)$, and the yz-plane, characterized by $(\psi = 90°|0° < \theta < 180°)$. The radiation pattern along the xz-plane exhibits a nearly directional distribution, emphasizing the antenna's performance in a specific angular range [25, 26]. On the other hand, the radiation pattern along the yz-plane provides additional perspectives on the antenna's emission characteristics, offering a comprehensive view of its spatial radiation behavior. This detailed analysis of the 2D radiation plot at the specified frequency contributes valuable insights into the antenna's directional emission patterns and aids in understanding its performance across different spatial planes [27].

Table 3 represents a significant step towards developing MPAs with enhanced bandwidth, catering to the evolving needs of modern communication and sensing technologies. The successful use of PAC ink opens new avenues for sustainable materials in radar applications, paving the way for further innovations in antenna design and materials science. The results of this study inspire further exploration and development in the quest for efficient and environmentally friendly wireless communication and radar systems [28].

6. CONCLUSION

This paper has successfully showcased a substantial improvement in the bandwidth of MPAs by employing a thick film based on PAC ink tailored explicitly for radar applications. The study encompassed the formulation and application of the conductive ink onto the MPA, followed by meticulous testing and analysis. The adoption of Prosopis Africana as a conductive material underscored its potential as an efficient and sustainable alternative and played a pivotal role in broadening the antenna's bandwidth. The obtained results, notably the observed augmentation in bandwidth, substantiate the effectiveness of Prosopis Africana conductive ink in augmenting MPA performance, thereby offering a promising avenue for radar applications. This research represents a noteworthy advancement in exploring environmentally friendly materials for radar technology, emphasizing the potential of Prosopis Africana in advancing Microstrip Patch Antennas in radar applications. Additionally, the successful fabrication of PAC thick film MPAs on an FR-4 substrate using the screen-printing technique signifies a valuable opportunity to exhibit the practical production of such antennas, anticipating favorable outcomes for the overall enhancement of antenna performance. The findings indicate commendable electrical properties of the PAC paste and MPA, with resistivity (ρ) measuring 0.2454 $|\Omega$/m and conductivity δ of 4.0750 S/m. Additionally, the antenna performance was evaluated, revealing a $|S_{11}|$ of -16.19 dB, operational across a bandwidth exceeding 1.85 GHz, achieving 84.5% radiation efficiency at operating frequency at 9.5 GHz and a peak realized gain of 7.1 dB. Thus, integrating PAC ink-based thick film emerges as a viable strategy for augmenting microstrip patch antenna bandwidth, making them more suitable for radar applications. The study contributes to the advancement of radar technology and aligns with the growing demand for environmentally conscious and sustainable electronic materials.

ACKNOWLEDGEMENT

This work was funded by the Petroleum Technology Development Fund (PTDF), Nigeria, and the Institute of Nanoscience and Nanotechnology (ION2), Universiti Putra Malaysia (UPM), Malaysia, and supported by Multimedia University (MMU) Cyberjaya R and D Malaysia.

REFERENCES

[1] Zhang, J. A., M. L. Rahman, K. Wu, X. Huang, Y. J. Guo, S. Chen, and J. Yuan, "Enabling joint communication and radar sensing in mobile networks — A survey," *IEEE Communications Surveys & Tutorials*, Vol. 24, No. 1, 306–345, 2022.

[2] Su, N., F. Liu, and C. Masouros, "Secure radar-communication systems with malicious targets: Integrating radar, communications and jamming functionalities," *IEEE Transactions on Wireless Communications*, Vol. 20, No. 1, 83–95, Jan. 2021.

[3] Balanis, C. A., *Antenna Theory: Analysis and Design*, John Wiley & Sons, 2016.

[4] Musa, U., S. Babani, S. A. Babale, A. S. Ali, Z. Yunusa, and S. H. Lawan, "Bandwidth enhancement of millimeter-wave microstrip patch antenna array for 5G mobile communication networks," *Bulletin of Electrical Engineering and Informatics*, Vol. 12, No. 4, 2203–2211, 2023.

[5] Palanivel Rajan, S. and C. Vivek, "Analysis and design of microstrip patch antenna for radar communication," *Journal of Electrical Engineering & Technology*, Vol. 14, 923–929, 2019.

[6] Musa, U., S. M. Shah, H. A. Majid, Z. Z. Abidin, M. S. Yahya, S. Babani, and Z. Yunusa, "Recent advancement of wearable reconfigurable antenna technologies: A review," *IEEE Access*, Vol. 10, 121 831–121 863, 2022.

[7] Anandkumar, D. and R. G. Sangeetha, "Design and analysis of aperture coupled micro strip patch antenna for radar applications," *International Journal of Intelligent Networks*, Vol. 1, 141–147, 2020.

[8] Babani, S., N. H. H. Khamis, B. D. Bala, and T. A. A. Mohammed, "A compact microstrip patch antenna for ADS-B operation," in *2014 IEEE Asia-Pacific Conference on Applied Electromagnetics (APACE)*, 250–252, 2014.

[9] Agboola, D. A., "Prosopis africana (Mimosaceae): Stem, roots, and seeds in the economy of the savanna areas of Nigeria," *Economic Botany*, Vol. 58, No. 1, S34–S42, 2004.

[10] Ogunshe, A., M. O. Omotosho, and A. D. V. Ayanshina, "Microbial studies and biochemical characteristics of controlled fermented afiyo-a nigerian fermented food condiment from prosopis africana (guill and perr.) taub," *Pakistan Journal of Nutrition*, Vol. 6, No. 6, 620–627, 2007.

[11] Akossou, A. Y. J., E. Gbozo, A. E. Darboux, and K. Kokou, "Influence of wood humidity of three species (Prosopis africana, Anogeissus leiocarpa and Tectona grandis) on the production of charcoal by the traditional wheel," *Journal of Petroleum Technology and Alternative Fuels*, 64–71, 2013.

[12] Bishop, B., F. B. P. Abang, and S. Attah, "Effect of fermentation with rumen content on the feeding value of boiled iron tree (prosopis africana) seedcoat on haematology and serum biochemistry of broiler chickens," *Annual Research & Review in Biology*, 70–77, 2021.

[13] Rahim, A. A. and Z. N. Garba, "Optimization of preparation conditions for activated carbon from Prosopis africana seed hulls using response surface methodology," *Desalination and Water Treatment*, Vol. 57, No. 38, 17 985–17 994, 2016.

[14] Nnamani, P. O., F. C. Kenechukwu, C. C. Okonkwo, and F. C. Otuu, "Performance of Prosopis Africana peel powder (PAPP) as a novel sorbent for remediating malachite green contaminated aqua system," *Scientific Research and Essays*, Vol. 7, No. 48, 4130–4137, 2012.

[15] Babani, S., M. N. Hamidon, I. Lawal, *et al.*, "Impact of micrometer and nanometer-sized particles on the electrical properties of prosopis africana biochar thick films," in *7th International Symposium on Advanced Materials and Nanotechnology (ISAMN2023)*, 2023.

[16] Hasan, I. H., M. N. Hamidon, A. Ismail, I. Ismail, A. S. Mekki, M. A. M. Kusaimi, S. Azhari, and R. Osman, "YIG thick film as substrate overlay for bandwidth enhancement of microstrip patch antenna," *IEEE Access*, Vol. 6, 32 601–32 611, 2018.

[17] Phadtare, V. D., V. G. Parale, G. K. Kulkarni, N. B. Velhal, H.-H. Park, and V. R. Puri, "Screen printed carbon nanotube thick film on alumina substrate," *Ceramics International*, Vol. 43, No. 5, 4612–4617, Apr. 2017.

[18] Ram, P., A. Yadav, M. K. Suman, and A. Kumar, "Graphene based circular shaped micro strip patch antenna array for 2.45 GHz ISM band application," *Wireless Personal Communications*, Vol. 116, 1613–1620, 2021.

[19] Kiflie, Z., M. Solomon, and S. K. Kassahun, "Statistically optimized charcoal production from prosopis juliflora for use as alternative fuel in cement factories," *Biomass Conversion and*

Biorefinery, 1–14, 2021.

[20] Shafiee, F. N., M. N. Hamidon, M. H. Wahid, A. H. Shaari, M. Ertugrul, N. H. Abdullah, M. A. M. Kusaimi, M. S. Mustaffa, I. H. Hasan, and I. R. Ibrahim, "Effect of nanometric and micronic particles size on physical and electrical properties of graphite thick film," *International Journal of Nanotechnology*, Vol. 17, No. 11-12, 825–839, 2020.

[21] Verma, A., A. K. Saxena, and D. C. Dube, "Microwave permittivity and permeability of ferrite-polymer thick films," *Journal of Magnetism and Magnetic Materials*, Vol. 263, No. 1-2, 228–234, 2003.

[22] Abadi, M. H. N. S., "Development of nanocrystalline thick film gas sensors," Ph.D. dissertation, Universiti Putra Malaysia, 2010.

[23] Sharma, A. and M. N. Afsar, "Microwave complex permeability and permittivity measurements of commercially available nanoferrites," *IEEE Transactions on Magnetics*, Vol. 47, No. 2, 308–312, 2010.

[24] Li, R., X. Yang, J. Li, Y. Shen, L. Zhang, R. Lu, C. Wang, X. Zheng, H. Chen, and T. Zhang, "Review on polymer composites with high thermal conductivity and low dielectric properties for electronic packaging," *Materials Today Physics*, Vol. 22, 100594, 2022.

[25] Muhammad, S., A. Smida, M. I. Waly, N. K. Mallat, A. Iqbal, S. R. Khan, and M. Alibakhshikenari, "Design of wideband circular-slot antenna for harvesting RF energy," *International Journal of Antennas and Propagation*, Vol. 2022, 5964753, 2022.

[26] Muhammad, S., J. J. Tiang, S. K. Wong, A. Smida, R. Ghayoula, and A. Iqbal, "A dual-band ambient energy harvesting rectenna design for wireless power communications," *IEEE Access*, Vol. 9, 99 944–99 953, 2021.

[27] Muhammad, S., J. J. Tiang, S. K. Wong, J. Nebhen, and A. Iqbal, "Design of a five-band dual-port rectenna for RF energy harvesting," *Computers Materials & Continua*, Vol. 69, No. 1, 487–501, 2021.

[28] Muhammad, S., J. J. Tiang, S. K. Wong, A. Iqbal, A. Smida, and M. K. Azizi, "A compact dual-port multi-band rectifier circuit for RF energy harvesting," *Computers Materials & Continua*, Vol. 68, No. 1, 167–184, 2021.

[29] Devi, K. S. C., B. Angadi, and H. M. Mahesh, "Multiwalled carbon nanotube-based patch antenna for bandwidth enhancement," *Materials Science and Engineering: B*, Vol. 224, 56–60, 2017.

[30] Syazwan, M. M., A. N. Hapishah, M. N. Hamidon, I. Ismail, and I. H. Hasan, "Design and development of Ni0. 75Zn0. 25Fe2O4/MWCNT microstrip patch antenna (MPA) for ISM band spectrum applications," *Synthetic Metals*, Vol. 271, 116630, 2021.

[31] Azman, I. Z. B., M. K. B. Othman, N. A. A. B. Zaini, and M. A. Jusoh, "Graphene-based materials for microstrip patch antenna," *Progress In Electromagnetics Research C*, Vol. 126, 207–216, 2022.

[32] Yunusa, Z. and A. A. Shehu, "Comparative study of single-slot and multi-slot graphene-based microstrip patch antenna for X-band application," *NanoEra*, Vol. 2, No. 1, 1–4, 2022.

[33] Shehu, A. A., Z. Yunusa, A. A. Gabari, and M. N. Hamidon, "Graphene based microstrip patch antenna using multiple slots for X and Ku band applications," in *AIP Conference Proceedings*, Vol. 2506, No. 1, 2022.

[34] Sa'don, S. N. H., M. H. Jamaluddin, M. R. Kamarudin, F. Ahmad, and S. H. Dahlan, "A 5G graphene antenna produced by screen printing method," *Indonesian Journal of Electrical Engineering and Computer Science*, Vol. 15, 950–1055, 2019.

[35] Wu, Y.-M., X. Lv, B. K. Tay, and H. Wang, "Carbon nanotube-based printed antenna for conformal applications," in *2013 International Conference on Optoelectronics and Microelectronics (ICOM)*, 91–93, 2013.

[36] Hasnat, T., S. M. A. Islam, S. H. Eshan, R. R. Hasan, J. Islam, and M. A. Rahman, "SWCNT based on-body antenna for detecting COVID-19 affected lung using 5G-band," in *2022 International Conference on Advancement in Electrical and Electronic Engineering (ICAEEE)*, 1–6, 2022.

[37] Német, A., S. Alkaraki, Q. H. Abassi, and S. F. Jilani, "A biodegradable textile-based graphene antenna for 5G wearable applications," in *2021 IEEE International Symposium on Antennas and Propagation and USNC-URSI Radio Science Meeting (APS/URSI)*, 1583–1584, IEEE, 2021.